Journal of Hazardous Materials 211–212 (2012) 188–195

Contents lists available at SciVerse ScienceDirect

Journal of Hazardous Materials

journal homepage: www.elsevier.com/locate/jhazmat

Cr(VI) photocatalytic reduction: Effects of simultaneous organics oxidation and of gold nanoparticles photodeposition on TiO_2

Maria Vittoria Dozzi, Alessia Saccomanni, Elena Selli*

Dipartimento di Chimica Fisica ed Elettrochimica and CIMAINA, Università degli Studi di Milano, via Golgi 19, I-20133 Milano, Italy

ARTICLE INFO

Article history:
Received 9 June 2011
Received in revised form 9 September 2011
Accepted 11 September 2011
Available online 16 September 2011

Keywords:
Photocatalytic reduction of Cr(VI)
Titanium dioxide
Au/TiO_2
Formic acid
Acid Orange 8

ABSTRACT

Commercial TiO_2 samples with different phase composition and surface area were tested as photocatalysts in the photoinduced reduction of Cr(VI) in aqueous suspensions at pH 3.7 under UV–visible light irradiation. This reaction was also coupled with the simultaneous photocatalytic oxidation of the pollutant azo dye Acid Orange 8 (AO8) and of formic acid, acting as hole scavengers. The co-presence of oxidizable and reducible species ensured better separation of photogenerated charge carriers, resulting in a higher rate of both organics' oxidation and Cr(VI) reduction, especially in the case of high surface area anatase TiO_2, having the strongest affinity for Cr(VI) and AO8, as demonstrated by competitive adsorption tests. The effects on Cr(VI) photocatalytic reduction of gold nanoparticles photodeposited on TiO_2 and of the Au loading were also investigated, aiming at ascertaining if this noble metal plays a role in the electron transfer processes involved in Cr(VI) reduction.

1. Introduction

The mobility and toxicity of aqueous chromium, a notoriously toxic, mutagenic and carcinogenic [1,2], common component of industrial wastes [3], depend on its oxidation state. Cr(VI), usually present in the form of highly soluble and toxic chromate anions, can efficiently be converted into Cr(III), which exhibits lower toxicity and mobility in the environment [4,5], by photocatalytic reduction on semiconductors [6–11]. When employing TiO_2, the most widely used semiconductor photocatalyst [12–14], this process is possible on the grounds of the energy level of the TiO_2 conduction band and of the reduction potential of the Cr(VI)/Cr(III) couple and it is favored at low pH. In fact, due to the three electrons involved in Cr(VI) reduction to Cr(III), the potential of this couple shifts to more positive values with decreasing pH with a slope higher than that of the conduction band edge shift with pH [11].

In order to investigate the influence of the surface and structural properties of this semiconductor on its photocatalytic activity, a series of commercial TiO_2 samples with different phase composition and surface area was tested in the photocatalytic reduction of Cr(VI) in aqueous suspensions at pH 3.7 under UV–visible light irradiation. This reaction was also coupled with the simultaneous photocatalytic oxidation of an organic pollutant, *i.e.* the azo dye Acid Orange 8 (AO8), see Scheme 1, and of formic acid, a small organic molecule undergoing direct photocatalytic mineralization to CO_2 and water, without the formation of any stable intermediate species.

Investigation on the simultaneous reduction and oxidation processes occurring under irradiation on the photocatalyst surface in contact with water not only provides valuable information on the rate of the electron transfer paths at work in the reaction system, but is of great importance in consideration of the fact that heavy metals, which can be photocatalytically reduced, and organic pollutants, which can be removed by photocatalytic oxidation, very often coexist in wastewaters. As outlined by Prairie et al. in their early study [8], an efficient design of photocatalytic systems for wastewater treatment must take into account both oxidation and reduction processes.

The photocatalytic reduction of Cr(VI) was already investigated in the presence of organics frequently present in natural and waste waters, such as humic substances [9], or pollutants, such as phenol and 4-chlorophenol [15–17], dyes [18–20], methyl *tert*-butyl ether [21], or carboxylic acids [17,22]. An increase in the rate of Cr(VI) photocatalytic reduction was usually observed. Most of these studies were performed employing the P25 TiO_2 photocatalyst and were mainly focused on the effects of substrates concentration and of pH. Our study is mainly focused on the effects of the TiO_2 phase composition and surface area on the rate of both Cr(VI) photocatalytic reduction and simultaneous oxidation of organic compounds, also in relation to their competitive adsorption on the photocatalyst surface.

Furthermore, the deposition of noble metals on semiconductor oxides is expected to enhance their photocatalytic activity by increasing the separation of photogenerated electron–hole pairs

* Corresponding author. Tel.: +39 02 503 14237; fax: +39 02 503 14300.
E-mail address: elena.selli@unimi.it (E. Selli).

0304-3894/$ – see front matter © 2011 Elsevier B.V. All rights reserved.
doi:10.1016/j.jhazmat.2011.09.038

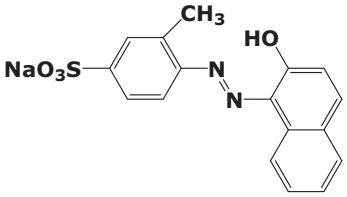

Scheme 1. Acid Orange 8 (AO8).

[23]. Indeed, the Fermi level of noble metals is usually lower in energy than the conduction band edge of TiO_2. Thus, photopromoted electrons can be captured by the noble metal, while photoproduced holes remain in the semiconductor valence band. However, whereas the positive effect of noble metal co-catalysts on the photocatalytic reduction processes, such as hydrogen production from water or O_2 reduction yielding hydrogen peroxide, is well established [24–26], their effective role in photocatalytic oxidative reactions is still under debate, especially in the case of gold-modified TiO_2 [27,28].

The effect on Cr(VI) photocatalytic reduction of gold nanoparticles photodeposited on the TiO_2 surface was also investigated in the present work and compared to their effect in the photocatalytic mineralization of formic acid. A series of TiO_2-based photocatalysts with different Au loadings were thus prepared and tested. The modifications induced on the photocatalyst surface by the noble metal photodeposition treatment were also taken into account.

2. Experimental

2.1. Materials and photocatalysts

Most chemicals, *i.e.* $K_2Cr_2O_7$, formic acid (FA), purity 95–97%, and Acid Orange 8 (AO8), were purchased from Aldrich. They were all employed as received, apart from AO8, which was purified by repeated crystallization from methanol, as already mentioned [29]. Water purified by a Milli-Q water system (Millipore) was used throughout.

Mixed phase Degussa P25 titanium dioxide (*ca.* 80% anatase, 20% rutile, surface area 48 $m^2\,g^{-1}$, according to our BET analysis [30]), and two pure anatase samples, purchased from Alfa Aesar, were employed as photocatalysts in powder form. These latter were labeled A118 and A235, with A standing for anatase, followed by a number indicating their surface area in $m^2\,g^{-1}$.

The series of gold-modified photocatalysts (Au/TiO_2) was prepared starting from 6 vol.% methanol/water suspensions, containing 3 $g\,L^{-1}$ of TiO_2 (Degussa P25) and the required amount of Au(III) acetate, as gold precursor, preliminary dissolved in an acidic aqueous medium. Au(III) photoreduction to metallic gold nanoparticles deposited on TiO_2 was achieved by irradiating the suspensions for 2 h under nitrogen atmosphere. An immersion fluorescent, low pressure mercury arc lamp (Jelosil) was employed as the irradiation source, emitting in the 300–400 nm range, with a maximum emission peak at 360 nm. Gold-modified TiO_2 powders were recovered after at least five centrifugation and washing cycles, up to the complete removal of residual ions and organic precursors. They were then dried at 70 °C for 1 day and stored in the absence of light and humidity. They were labeled with P, standing for "photodeposited", followed by their nominal gold content, in weight percent. A reference sample (P 0%) was prepared following exactly the same procedure, except for the addition of the gold precursor.

2.2. Photocatalysts characterization

UV–vis diffuse reflectance (DR) spectra were recorded with a Lambda 19, Perkin Elmer spectrophotometer equipped with an integrating sphere. HRTEM images were obtained with a JEM 3010 (JEOL) electron microscope operating at 300 kV. XPS analyses were performed by a PHI-5500-Physical Electronics spectrometer, equipped with a monochromatized source with aluminum anode (K_α = 1486.6 eV). XRD analysis was performed employing a Philips PW 1820 power diffractometer, using filtered Cu Kα radiation. The BET surface area was measured by nitrogen adsorption/desorption at 77 K employing a Micromeritics ASAP 2010 apparatus. All these characterization measurements were performed on the photocatalysts employed in this work, following the operating conditions and procedures already described in detail [31].

2.3. Photocatalytic and adsorption tests

All photocatalytic runs were performed in aqueous suspensions under atmospheric conditions, in a magnetically stirred 100 mL reactor, inserted in a home made housing consisting in a black box mounted on optical bench [31]. The irradiation source was an Osram, model Powerstar HCI-T, 150 W/NDL lamp, mounted on a Twin Beam T 150 R reflector, mainly emitting visible light above 400 nm, with a small emission in the 350–400 nm range (see Fig. 6 of Ref. [31]) and an average full emission intensity on the reactor of 2.5×10^{-7} Einstein $s^{-1}\,cm^{-2}$, as periodically checked by ferrioxalate actinometry. A 285 nm cut off filter was mounted at the black box entrance. The lamp and the reactor were separated by a fixed distance of 10 cm. The whole set up was maintained at ambient temperature by a continuous stream of air.

All irradiated aqueous suspensions contained 0.1 $g\,L^{-1}$ of photocatalyst. The photocatalysts dispersed in pure water were preliminarily sonicated in a Eurosonic, Model 22, apparatus for 30 min. Then appropriate volumes of stock solutions containing Cr(VI), Acid Orange 8 (AO8) or formic acid (FA) were added. The initial concentration of the photocatalytic reaction substrates in the aqueous suspensions were fixed at the following values: 3.3×10^{-5} M for Cr(VI), from a solution obtained by dissolving $K_2Cr_2O_7$ in water, and 1.0×10^{-3} M for FA, 2.8×10^{-5} M for AO8. Before starting irradiation, the so obtained suspensions were magnetically stirred in the dark for 15 min to attain the adsorption equilibrium of the substrates on the photocatalyst surface.

Stirring was continued during the runs. The lamp was always switched on at least 30 min before the beginning of irradiation. At different time intervals during the runs, 3-mL samples of the suspension were withdrawn from the reactor and centrifuged employing a EBA-20 Hettich centrifuge. The supernatant was analyzed colorimetrically for Cr(VI) residual content, using the 1,5-diphenylcarbazide method [32]. AO8 photobleaching was monitored during the runs by spectrophotometric analysis at the wavelength of maximum AO8 absorption, *i.e.* 490 nm. The molar extinction coefficient of the dye at this wavelength is $\varepsilon = (3.06 \pm 0.02) \times 10^4\,M^{-1}\,cm^{-1}$, according to previous calibration [29]. FA content in the supernatant was determined by ion chromatography with conductivity detection, employing a Metrohm 761 Compact IC instrument [31], as already described, after calibration for formate ion concentration in the 0–50 ppm range.

All kinetic runs were performed up to *ca.* 70% Cr(VI) removal and repeated at least twice, to check their reproducibility. The initial pH of the suspensions was fixed at pH 3.7 by addition of the appropriate volume of a concentrated $HClO_4$ solution. No addition was necessary in the case of FA-containing suspensions, because 3.7 was the natural pH of the aqueous suspensions containing 1.0×10^{-3} M FA. The pH of the suspension was measured before and after each run by means of an Amel, model 2335 pH-meter; no significant pH variation occurred during the runs.

Aiming at investigating the substrates affinity for the different photocatalysts, adsorption tests were performed at pH 3.7 under the same initial conditions of the photocatalytic runs, except for the

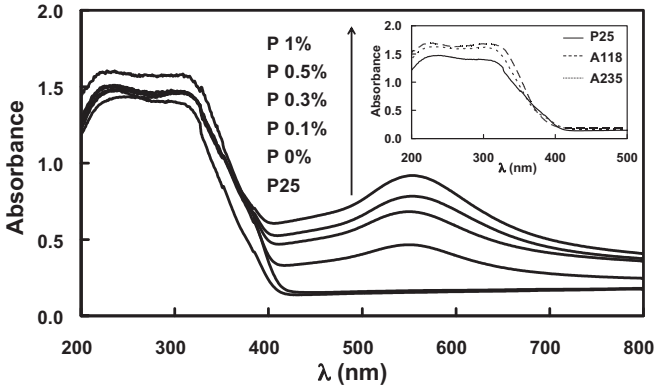

Fig. 1. Absorption spectra of P25 TiO_2 and of the Au/TiO_2 photocatalysts series, with increasing Au loading, prepared by photodeposition. Inset: absorption spectra of P25, A118 and A235.

amount of TiO_2, which was fixed at 1.0 g L^{-1}. The suspensions were kept under stirring in the dark and samples were withdrawn after 30 min, 1 h, 6 h and 24 h, centrifuged and analyzed for the Cr(VI) and/or AO8 amount in the supernatant. Adsorption equilibrium was attained in 30 min.

3. Results and discussion

3.1. Photocatalysts characterization

XRD analysis confirmed the mixed phase composition of Degussa P25, with a 78:22 anatase-to-rutile ratio, and mean diameter of the anatase and rutile crystallites of 25 ± 5 and 35 ± 8 nm, respectively [30]. Also the composition (pure anatase) of the A118 and A235 samples was confirmed by XRD analysis; the mean diameter of crystallites was 18 ± 3 and 9 ± 1 nm, respectively.

These TiO_2 samples exhibit quite similar absorption properties, with an absorption onset around 400 nm, according to UV–vis DR measurements. In comparison to the pure anatase samples, P25 exhibits a slightly red-shifted absorption edge (see Fig. 1, inset), due to the presence of the rutile phase, characterized by a smaller band gap value (*i.e.* 3.0 eV *vs.* 3.2 eV for anatase).

As shown in Fig. 1, all Au/TiO_2 samples exhibited the typical plasmon resonance band of gold nanoparticles (<20 nm), centered at 550 nm, *i.e.* red shifted compared to the pure gold plasmonic peak (520 nm), indicating interaction between gold and the titania support. The intensity of the plasmon resonance band regularly increased with increasing the gold loading without any appreciable difference in the absorption maximum (Fig. 1), indicating a progressive increase in gold nanoparticles density on the oxide surface without marked variation of their dimensions.

HRTEM analysis yielded direct information on the dimension and the distribution of Au nanoparticles. Examples of HRTEM images are reported in Fig. 2. The mean diameter of gold nanoparticles obtained by photoreduction varied between 5 and 20 nm. Compared to other gold deposition techniques (*e.g.* the deposition-precipitation method [31]), photodeposition was reported to produce larger and more spherical noble metal nanoparticles [33].

No variation in XRD patterns was expected after gold deposition by the adopted photodeposition procedure, not implying any heat treatment, as already verified in previous studies [31,34]. Also the specific surface area of P25 TiO_2 did not vary upon gold nanoparticles deposition, in line with analogous results obtained by us [31] and by other research groups [35–37].

The XPS analysis of the surface chemical composition, reported in Table 1, confirmed that all samples maintained a O/Ti atom ratio very close to 2, indicating no variation in the metal oxide surface composition, and confirmed the presence of gold nanoparticles deposited on the Au/TiO_2 photocatalysts. The gold percent surface amount detected by XPS analysis regularly increased with increasing the nominal gold loading of the samples prepared by photodeposition. Furthermore, XPS analysis did not evidence any significant variation of chlorine content and of adventitious surface carbon content with respect to the values detected for pristine P25 TiO_2, indicating negligible persistence of Cl^- ions or of organic substances originating from the gold precursor.

3.2. Cr(VI) photocatalytic reduction tests on TiO_2

The photocatalytic reduction of Cr(VI) occurred according to a first order rate law in the presence of both TiO_2 and Au/TiO_2 photocatalysts. Determination coefficients R^2 obtained by treating the Cr(VI) concentration *vs.* time data according to a first order rate law were always greater than 0.98. The photoactivity of different photocatalyst powders was thus compared in terms of first order rate constants of Cr(VI) reduction obtained under identical irradiation conditions in the presence of an equal photocatalyst amount (0.1 g L^{-1}).

The effect of pH was preliminarily investigated employing P25-containing suspensions, in order to attain optimal Cr(VI) photoreduction conditions. The rate constant of Cr(VI) photocatalytic reduction at the natural pH conditions of the dichromate suspension, *i.e.* pH *ca.* 6.5, was $(8.2 \pm 0.8) \times 10^{-5}$ s^{-1}, whereas an almost doubled rate constant, *i.e.* $(1.61 \pm 0.05) \times 10^{-4}$ s^{-1}, was determined employing a suspension at pH 3.7, obtained by $HClO_4$ addition. All subsequent runs were thus performed at this pH. This result is in agreement with previous findings of different laboratories and is expected from the already mentioned shift of potentials with decreasing pH [8,11,12,38–40].

The photocatalytic activity of the different bare TiO_2 samples investigated in the present work can be compared in Fig. 3, in terms

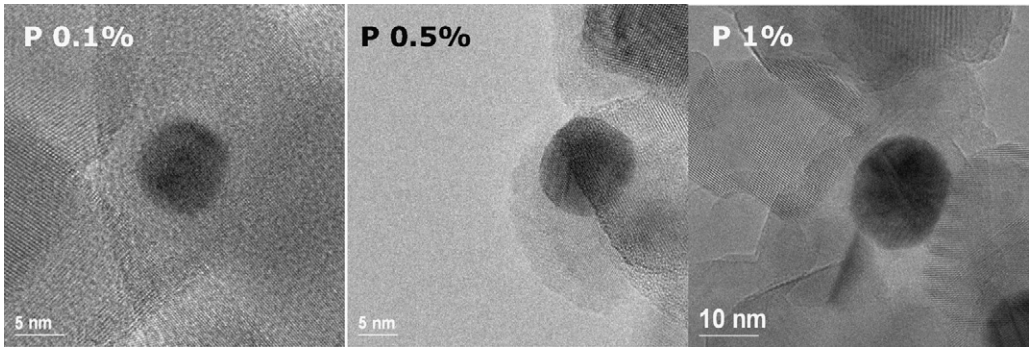

Fig. 2. HRTEM images of selected Au/TiO_2 samples.

Table 1
Surface composition, from XPS analysis, of P25 TiO_2 and of Au/TiO_2 photocatalysts prepared by photodeposition of different percent amounts of gold nanoparticles.

Au/TiO_2 sample	Atom %				
	C 1s	O 1s	Ti 2p	Cl 2p	Au 4f
P25	14.1	55.9	28.0	0.8	–
P 0%	16.2	54.5	27.4	0.6	–
P 0.1%	15.6	54.8	27.7	0.6	0.06
P 0.3%	16.8	54.0	26.7	0.7	0.12
P 0.5%	15.8	54.2	27.4	0.8	0.16
P 1%	16.4	54.4	26.3	0.7	0.21

of first order rate constants of Cr(VI) reduction. Their uncertainties, obtained from repeated runs, are also shown in the figure. P25 TiO_2 was found to be the best performing photocatalyst, followed by A118 and by A235. The rate of Cr(VI) reduction thus appears totally independent of the photocatalyst surface area, but rather limited by the intrinsic efficiency in photoproduced charges separation of the employed photocatalyst powder. P25 TiO_2, manufactured by flame hydrolysis of titanium tetrachloride at high temperature, exhibits outstanding photocatalytic activity in several reactions, to be attributed to its peculiar nanostructured arrangement of interwoven anatase-rutile crystallites hindering charge recombination by charge separation across interfaces [41,42].

3.3. Effect of AO8 on Cr(VI) adsorption and photocatalytic reduction on TiO_2

Preliminary tests of Cr(VI) and AO8 equilibrium adsorption on the investigated photocatalysts were performed at pH 3.7 under the same conditions employed in photocatalytic runs, except for a 10-fold higher amount of TiO_2.

The percent amount of Cr(VI) adsorbed on the photocatalysts, both in the presence and in the absence of AO8, is shown in Fig. 4. The adsorption of Cr(VI), present in the suspensions in the form of negatively charged $Cr_2O_7^{2-}$ ions, clearly increased with increasing the surface area of the TiO_2 photocatalysts. The extent of Cr(VI) adsorption on all photocatalysts was lower in the presence of the azo dye, indicating competitive adsorption. Indeed, at pH 3.7 both AO8 and Cr(VI) are in the anionic form, whereas the TiO_2 surface is positively charged, its point of zero charge being at pH higher than 3.7.

The extent of AO8 equilibrium adsorption on the photocatalysts was also measured, both in the presence and in the absence of Cr(VI). The results shown in Fig. 5 demonstrate that AO8 largely adsorbed on the TiO_2 photocatalysts, and that the adsorbed amount was also larger on higher surface area photocatalysts. The fact that AO8 adsorption occurred in competition with dichromate adsorption was confirmed by the lower AO8 adsorption extent attained

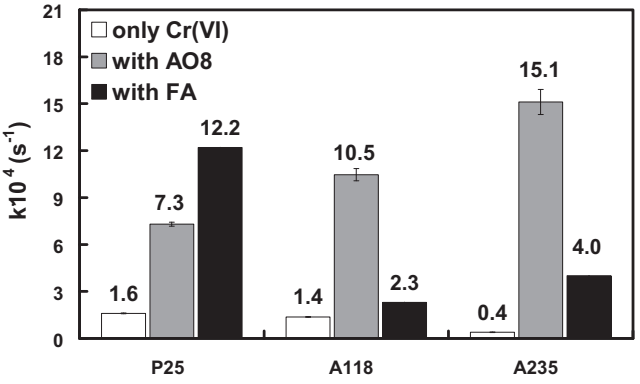

Fig. 3. Rate constants of Cr(VI) photocatalytic reduction in the absence of organics and in the presence of the azo dye AO8 and of formic acid (FA).

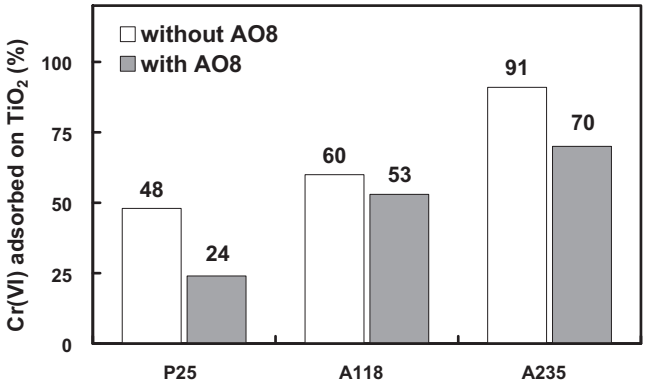

Fig. 4. Percent amount of Cr(VI), in the form of dichromate anion, adsorbed at equilibrium on TiO_2 photocatalysts (1.0 g L^{-1}), in the absence and in the presence of the AO8 azo dye. Overall Cr(VI) concentration: 3.3×10^{-5} M; overall AO8 concentration: 2.8×10^{-5} M.

in the presence of Cr(VI) (Fig. 5). The effects of competitive adsorption were more pronounced in the case of P25 photocatalyst, as expected, due to its lower specific surface area (Figs. 4 and 5).

The simultaneous presence of Cr(VI) and of the azo dye AO8, undergoing photocatalytic oxidation under irradiation, led to a marked enhancement of the rate of Cr(VI) photoreduction, which was clearly higher for photocatalysts with higher surface area (see Fig. 3). Similar results were obtained in the presence of other organics, *e.g.* methyl *tert*-butyl ether [21], different dyes [18–20] or carboxylic acids [17,22].

The dye itself was found to undergo photocatalytic oxidation according to a first order rate law, both in the presence and in the absence of Cr(VI). In both cases the photocatalytic bleaching of the dye increased with increasing the surface area of the photocatalyst, as shown in Fig. 6. Furthermore, AO8 photodegradation was markedly enhanced by the simultaneous presence of Cr(VI) and

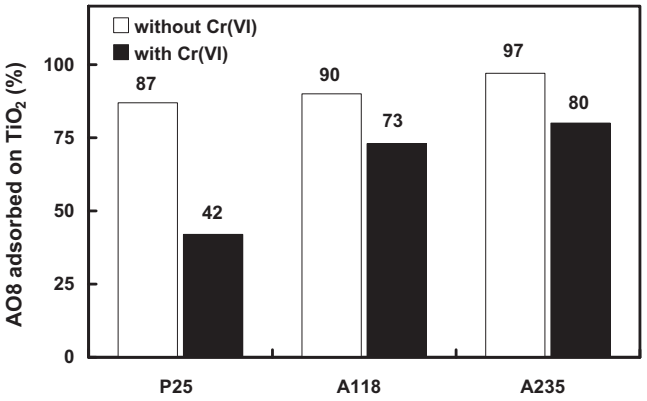

Fig. 5. Percent amount of AO8 adsorbed at equilibrium on TiO_2 photocatalysts (1.0 g L^{-1}), in the absence and in the presence of Cr(VI) as dichromate anion. Overall AO8 concentration: 2.8×10^{-5} M; overall Cr(VI) concentration: 3.3×10^{-5} M.

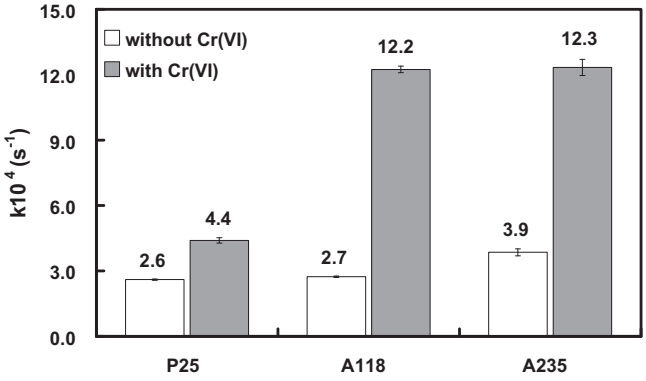

Fig. 6. Rate constants of AO8 photocatalytic oxidation in the absence and in the presence of Cr (VI).

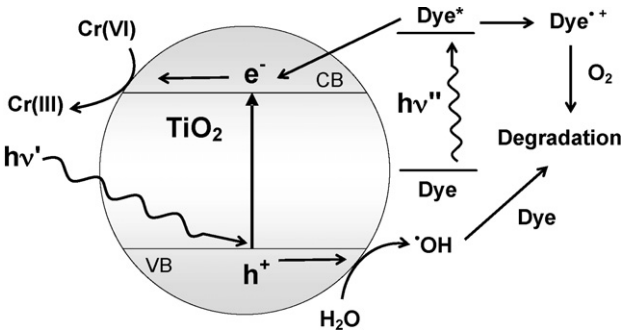

Scheme 2. Dye-sensitized and band gap absorption-initiated paths of simultaneous Cr(VI) reduction and AO8 oxidation.

this effect was more remarkable for the two high surface area pure anatase photocatalysts (Fig. 6).

Aromatic azo dyes undergo photocatalytic bleaching through an oxidation mechanism mainly involving hydroxyl radicals, which upon band gap excitation are photocatalytically generated on the oxide surface from the oxidation of surface –OH groups or water molecules. These radicals attack the diazo moiety, leading to loss of visible light absorption [43–46]. This occurs on the photocatalyst surface, the hydroxyl radicals being unable to leave it [47]. Consequently this oxidation path is largely favored by substrate adsorption on the photocatalyst surface. In fact, both in the presence and in the absence of Cr(VI) the rate of AO8 photocatalytic oxidation increased with the surface area of the employed photocatalyst (Fig. 6), on which a larger percent amount of dye could adsorb (Fig. 5). The simultaneous photooxidation of the organic dye clearly had a synergistic effect in Cr(VI) reduction, and this effect was greater, the larger was the surface area of the photocatalyst (Fig. 3).

In fact, the photocatalytic activity in Cr(VI) reduction in the absence of AO8 did not increase with increasing the photocatalyst surface area, because it mainly depends on the intrinsic efficiency of electron–hole separation, as stated above. However, the simultaneous presence of Cr(VI) and AO8 led to an enhancement of the photocatalytic activity, which was clearly higher for photocatalysts with higher specific surface area, *i.e.* for photocatalysts on which AO8 underwent faster degradation. Indeed, photopromoted conduction band electrons became more readily available for Cr(VI) reduction in the presence of AO8, which indirectly consumed photoproduced valence band holes and thus inhibited electron–hole recombination. Therefore, the co-presence of oxidizable and reducible species ensured better separation of photogenerated charge carriers, especially in the case of high surface area anatase TiO_2, having the strongest affinity for both degradation substrates, as demonstrated by competitive adsorption tests.

Concerning the mechanistic aspects of Cr(VI) photocatalytic reduction, the reaction was shown to occur through a sequence of one electron transfer steps and experimental evidence was obtained of the involvement of Cr(V) in the form of aquo and EDTA complex [48,49]. When the reaction was combined with the photocatalytic oxidation of an organic species able itself to absorb light, such as the azo dye AO8 in the present study, absorbing a considerable portion of visible light under the adopted irradiation conditions, a sensitized mechanism might be at work, in parallel to that initiated by semiconductor band gap absorption. In fact, as shown in Scheme 2, the electronically excited state of the dye, produced by visible light absorption, is able to transfer electrons into the conduction band of TiO_2 or to adsorbed Cr(VI), producing a dye radical cation, which easily undergoes oxidation by O_2 molecules. Such reaction path is responsible for the visible light-induced photocatalytic reduction of Cr(VI) in the presence of dyes [20] and is perfectly compatible with the surface area and adsorption dependence observed for the rate of both oxidation and reduction reactions simultaneously occurring on the photocatalyst surface.

In contrast, present photocatalytic activity results, clearly dependent on the surface area of the employed photocatalyst, seem to exclude that the enhanced Cr(VI) photoinduced reduction observed in the presence of AO8 occurred through direct electron transfer from AO8 to Cr(VI) in a AO8–Cr(VI) complex in the aqueous phase, as suggested to occur in the case of the azo dye Acid Orange 7 [20]. In fact, both Cr(VI) and AO8 were found to be perfectly photostable in aqueous solutions containing no TiO_2, even after prolonged irradiation under the conditions employed in the present study. Similar Cr(VI) complexes were shown to play a role in the photocatalytic Cr(VI) reduction in the presence of, *e.g.*, salicylic and citric acids [20,22,50].

On the other hand, evidence was recently obtained of the formation of a charge transfer complex between Cr(VI) and TiO_2 [51] that could be excited by visible light. The efficiency of Cr(VI) reduction attained by selectivity exciting this complex was found to be higher than that produced by exciting the semiconductor itself. An electron transfer path initiated by this way cannot be excluded to be at work under the irradiation conditions of the present work.

3.4. Effect of formic acid on Cr(VI) photocatalytic reduction

Aiming at excluding the possibility of any dye-sensitized photocatalytic reaction path, we investigated the effect of the presence of formic acid in the photocatalytic reduction of Cr(VI). This acidic organic substrate does not absorb light in competition with TiO_2 and is known to undergo photocatalytic oxidation mainly through direct interaction with photoproduced valence band holes [43,46,52], without forming any stable mineralization intermediate.

The effect of FA addition on the rate of Cr(VI) photocatalytic reduction is also shown in Fig. 3 and can be easily compared with that of AO8 addition in the irradiated suspensions. The rate of Cr(VI) photoreduction was clearly higher in the presence of both organic species, with respect to the rate measured in the absence of any organics. However, the photoactivity trend within the investigated photocatalyst series obtained after FA addition was completely different with respect to that observed after AO8 addition. In fact, a remarkable rate increase was obtained upon FA addition when employing P25 TiO_2, whereas FA addition had much smaller effects on Cr(VI) reduction rate in the case of the two high surface area pure anatase photocatalysts, the photoactivity of which markedly increased upon AO8 addition. Thus Cr(VI) reduction in the presence of a direct hole scavenger, such as FA, appears to be still limited

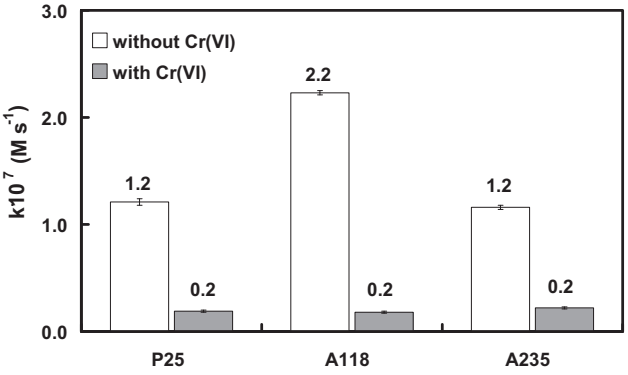

Fig. 7. Zero-order rate constants of FA photocatalytic oxidation in the absence and in the presence of Cr (VI).

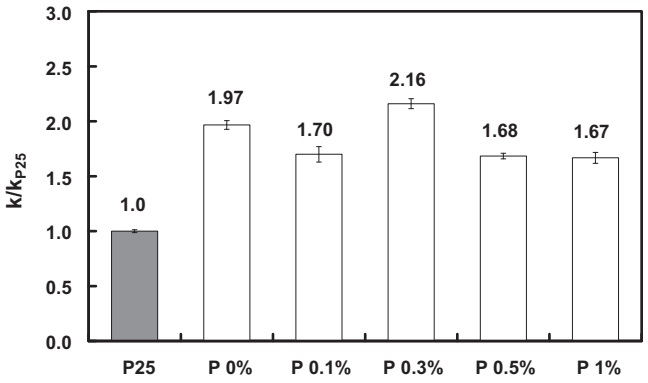

Fig. 8. Effect of gold nanoparticles photodeposited on TiO_2 on the photocatalytic reduction of Cr(VI): ratio between the first order rate constants k measured in the presence of Au/TiO_2 samples with different gold loading (wt.%) and that obtained with unmodified P25, k_{P25}.

by the electron–hole separation intrinsic properties of the semiconductors, rather than by effects related to their surface area and substrate adsorption capability.

Simultaneous to Cr(VI) photocatalytic reduction, FA underwent photocatalytic mineralization at constant rate, *i.e.* according to a zero-order rate law, as already observed in previous studies [31,46,52]. Fig. 7 shows that pure anatase A118 was the best performing photocatalyst in FA mineralization in the absence of Cr(VI). Comparable results were obtained under UV irradiation [30]. However, the rate of FA mineralization dramatically dropped when Cr(VI) was added to the irradiated suspensions, down to a rather low value, almost independent of the employed TiO_2 photocatalyst (Fig. 7). Very low FA conversion (below 10%) was attained in this case at the end of the runs. This effect could not be attributed to Cr(VI)–FA interactions in the aqueous phase, because aqueous solutions containing both Cr(VI) and FA at pH 3.7 were found to be perfectly stable both in the absence and in the presence of irradiation, in contrast to previous studies carried out under intense UV irradiation [53].

It is worth noting, however, that the initial FA concentration in our suspensions was more than one order of magnitude higher than the initial Cr(VI) concentration and that the rate of FA oxidation, coinciding with the zero-order rate constants values of Fig. 7, was similar to the rate of Cr(VI) photocatalytic reduction in the presence of FA, calculated as $r = k$ [Cr(VI)], k being the first order rate constants reported in Fig. 3 for Cr(VI) reduction in the presence of FA. Thus the photocatalytic oxidation and reduction processes proceeded at almost the same rate on the photocatalysts surface. This rate was lower than the rate of FA oxidation in the absence of Cr(VI), indicating that chromium species adsorbed on the photocatalyst surface inhibit FA photocatalytic oxidation. Indeed, previous studies on Cr(VI) photocatalytic reduction in the presence of carboxylic acids evidenced an inhibition in TOC degradation [50] or even an increase of TOC amount [22] during the photocatalytic runs, which were attributed to deactivation of the photocatalyst surface due to Cr(III) adsorption or to desorption of organic species from the photocatalyst surface under irradiation, respectively. This chromium-induced inhibition in the photocatalytic mineralization of organics should deserve attention, because it may cause problems in the photocatalytic treatment of waste waters.

3.5. Effect of gold nanoparticles deposition on TiO_2

The effects induced on the rate of Cr(VI) reduction by the presence of gold nanoparticles photodeposited on the surface of P25 TiO_2 can be appreciated in Fig. 8, where the first order rate constants obtained with the Au/TiO_2 photocatalysts series are reported as normalized values with respect to the rate constant value k_{P25} obtained with unmodified P25 TiO_2. Also with the Au/TiO_2 photocatalysts, Cr(VI) photoreduction became faster upon FA addition to the irradiated suspensions, with an average 4-fold increase of the rate constants of Cr(VI) reduction (data not shown).

The photocatalytic activity scale of the Au/TiO_2 samples in FA oxidation can be appreciated in Fig. 9, showing the ratios between the zero-order rate constants of FA degradation obtained with each photocatalyst and that measured in the presence of unmodified P25. On the other hand, FA oxidation rate dropped to very low values in the presence of Cr(VI), in a way almost identical to that shown in Fig. 7 in the case of the unmodified photocatalysts.

The presence of photodeposited gold nanoparticles had a beneficial role primarily in increasing the rate of FA oxidation (Fig. 9). The photoactivity increase obtained by gold photodeposition was slightly higher than that obtained with gold-modified TiO_2 prepared according to the deposition-precipitation method [31] and can be attributed to the formation of the carbon dioxide radical anion upon the one electron oxidation of FA. In fact, such strongly reductant species may contribute in maintaining gold in its photocatalytically active metallic form, avoiding the possible formation of Au^+ by Au(0) interaction with conduction band holes [31]. Furthermore, the photodeposition procedure itself, even in the absence of gold precursor, slightly increased the photoactivity of P25 (see P 0% *vs.* P25 in Fig. 9).

The rate enhancement observed in the case of Cr(VI) photocatalytic reduction upon loading P25 TiO_2 with gold nanoparticles shows an unclear trend as a function of metal loading. Also

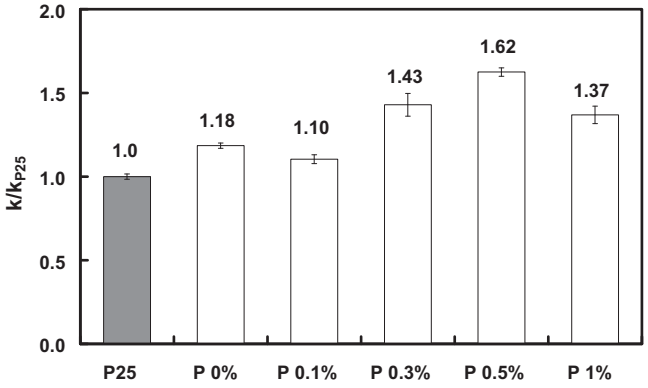

Fig. 9. Effect of gold nanoparticles photodeposited on TiO_2 on the photocatalytic oxidation of FA: ratio between the zero-order rate constants k measured in the presence of Au/TiO_2 samples with different gold loading (wt.%) and that obtained with unmodified P25, k_{P25}.

in this case the photodeposition procedure produced positive effects on P25 photoactivity, which were even greater than in FA photocatalytic degradation. In fact, the rate constant of Cr(VI) photoreduction almost doubled when P25 TiO_2 was pre-irradiated under anaerobic conditions in the absence of gold precursor (see k/k_{P25} of P 0% in Fig. 8), most probably as a consequence of the partial TiO_2 surface reduction, whereas metal loading did not exhibit a definite effect. The improvement of the photocatalytic efficiency of these Au/TiO_2 materials in Cr(VI) reduction should thus be attributed more to partial TiO_2 reduction than to the presence of gold nanoparticles. Indeed, rather small effects of noble metals on the rate of Cr(VI) photocatalytic reduction were reported in the literature, for example in the case of mesoporous titania photocatalysts embedding gold nanoparticles [54], whereas platinization of titania was found to produce no improvement in its photoactivity in Cr(VI) reduction [55].

The rate of both photocatalytic oxidation and reduction reactions were found to slightly vary with metal loading, attaining a maximum value for the P 0.3% photocatalyst in the case of Cr(VI) reduction (Fig. 8) and for P 0.5% in the case of FA oxidation (Fig. 9), *i.e.* for a 0.5 wt.% gold loading, as in previous studies [31]. These maximum reaction rates were attained for an optimal balance between the detrimental shielding effects of Au surface nanoparticles, decreasing the fraction of light absorbed by TiO_2, and their beneficial role in capturing conduction band electrons, thus reducing the recombination of photoproduced electron–hole couples. Present results demonstrate that, when discussing the modifications in Cr(VI) reduction photoactivity induced by the presence of noble metal nanoparticles on the photocatalyst surface, the effects induced by the deposition procedure should be clearly distinguished from those induced by noble metal nanoparticles themselves.

Acknowledgements

The collaboration of Dr. Laura Meda, Istituto ENI Donegani, Novara, in XPS analysis and of Dr. Patrizia Canton, Università di Venezia, in HRTEM analysis is gratefully acknowledged. This work received financial support from the Cariplo Foundation through the project *Development of Second Generation Photocatalysts for Energy and Environment*.

References

[1] J.A.H. Waterhouse, Cancer among chromium platers, Br. J. Cancer 32 (1975) 262–267.
[2] C.D. Palmer, P.R. Wittbrodt, Processes affecting the remediation of chromium-contaminated sites, Environ. Health Perspect. 92 (1991) 25–40.
[3] U. Förster, G.T.W. Wittmann (Eds.), Metal Pollution in Aquatic Environment, 2nd ed., Springer-Verlag, New York, 1983.
[4] V. Bianchi, A. Zantedeschi, A. Montaldi, J. Majone, Trivalent chromium is neither cytotoxic nor mutagenic in permeabilized hamster fibroblasts, Toxicol. Lett. 8 (1984) 279–286.
[5] S. Music, M. Ristic, M. Tonkovic, Sorption of chromium(VI) on hydrous iron-oxides, Z. Wasser Abwass. Forsch. 19 (1986) 186–196.
[6] H. Yoneyama, Y. Yamashita, H. Tamura, Heterogeneous photocatalytic reduction of dichromate on n-type semiconductor catalysts, Nature 281 (1979) 817–818.
[7] J. Muñoz, X. Doménech, TiO_2 catalysed reduction of Cr(VI) in aqueous solutions under ultraviolet illumination, J. Appl. Electrochem. 20 (1990) 518–521.
[8] M.R. Prairie, L.R. Evans, B.M. Stange, S.L. Martinez, An investigation of TiO_2 photocatalysis for the treatment of water contaminated with metals and organic chemicals, Environ. Sci. Technol. 27 (1993) 1776–1782.
[9] E. Selli, A. De Giorgi, G. Bidoglio, Humic acid-sensitized photoreduction of Cr(VI) on ZnO particles, Environ. Sci. Technol. 30 (1996) 598–604.
[10] J. Giménez, M.A. Aguado, S. Cervera-March, Photocatalytic reduction of Cr(VI) with titania powders in a flow system. Kinetics and catalyst activity, J. Mol. Catal. A: Chem. 105 (1996) 67–78.
[11] X. Wang, S.O. Pehkonen, A.K. Ray, Removal of aqueous Cr(VI) by combination of photocatalytic reduction and coprecipitation, Ind. Eng. Chem. Res. 43 (2004) 1665–1672.
[12] M.I. Litter, Heterogeneous photocatalysis. Transition metal ions in photocatalytic systems, Appl. Catal. B: Environ. 23 (1999) 89–114.
[13] X. Chen, S.S. Mao, Titanium dioxide nanomaterials: synthesis, properties, modifications, and applications, Chem. Rev. 107 (2007) 2891–2959.
[14] A. Fujishima, X. Zhang, D.A. Tryk, TiO_2 photocatalysis and related surface phenomena, Surf. Sci. Rep. 63 (2008) 515–582.
[15] H. Fu, G. Lu, S. Li, Adsorption and photo-induced reduction of Cr(VI) ion in Cr(VI)–4CP(4-chlorophenol) aqueous system in the presence of TiO_2 as photocatalyst, J. Photochem. Photobiol. A: Chem. 114 (1998) 81–88.
[16] S.M. Lee, T.W. Lee, B.J. Choi, J.K. Yang, J. Environ. Sci. Health A 38 (2003) 2219–2228.
[17] L. Wang, N. Wang, L. Zhu, H. Yu, H. Tang, Photocatalytic reduction of Cr(VI) over different TiO_2 photocatalysts and the effects of dissolved organic species, J. Hazard. Mater. 152 (2008) 93–99.
[18] S.G. Schrank, H.J. José, R.F.P.M. Moreira, Simultaneous photocatalytic Cr(VI) reduction and dye oxidation in a TiO_2 slurry reactor, J. Photochem. Photobiol. A: Chem. 147 (2002) 71–76.
[19] T. Papadam, N.P. Xekoukoulotakis, I. Poulios, D. Mantzavinos, Photocatalytic transformation of acid orange 20 and Cr(VI) in aqueous suspensions, J. Photochem. Photobiol. A: Chem. 186 (2007) 308–315.
[20] H. Kyung, J. Lee, W. Choi, Simultaneous and synergistic conversion of dyes and heavy metal ions in aqueous TiO_2 suspensions under visible-light illumination, Environ. Sci. Technol. 39 (2005) 2376–2382.
[21] X.R. Xu, H.B. Li, J.D. Gu, Simultaneous decontamination of hexavalent chromium and methyl *tert*-butyl ether by UV/TiO_2 process, Chemosphere 63 (2006) 254–260.
[22] G. Colón, M.C. Hidalgo, J.A. Navío, Influence of carboxylic acid on the photocatalytic reduction of Cr(VI) using commercial TiO_2, Langmuir 17 (2001) 7174–7177.
[23] P.V. Kamat, Photophysical, photochemical and photocatalytic aspects of metal nanoparticles, J. Phys. Chem. B 106 (2002) 7729–7744.
[24] C.M. Wang, A. Heller, H. Gerischer, Palladium catalysis of O_2 reduction by electrons accumulated on TiO_2 particles during photoassisted oxidation of organic compounds, J. Am. Chem. Soc. 114 (1992) 5230–5234.
[25] A.L. Linsebigler, G. Lu, J.T. Yates Jr., Photocatalysis on TiO_2 surfaces: principles, mechanisms, and selected results, Chem. Rev. 95 (1995) 735–758.
[26] G.L. Chiarello, E. Selli, L. Forni, Photocatalytic hydrogen production over flame spray pyrolysis-synthesised TiO_2 and Au/TiO_2, Appl. Catal. B: Environ. 84 (2008) 332–339.
[27] S.L. Lee, J. Scott, K. Chiang, R. Amal, Nanosized metal deposits on titanium dioxide for augmenting gas-phase toluene photooxidation, J. Nanopart. Res. 11 (2009) 209–219.
[28] B.K. Min, J.E. Heo, N.K. Youn, O.S. Joo, H. Lee, J.H. Kim, H.S. Kim, Tuning of the photocatalytic 1,4-dioxane degradation with surface plasmon resonance of gold nanoparticles on titania, Catal. Commun. 10 (2009) 712–715.
[29] E. Selli, Synergistic effects of sonolysis combined with photocatalysis in the degradation of an azo dye, Phys. Chem. Chem. Phys. 4 (2002) 6123–6128.
[30] C. Bernardini, G. Cappelletti, M.V. Dozzi, E. Selli, Photocatalytic degradation of organic molecules in water: photoactivity and reaction paths in relation to TiO_2 particles features, J. Photochem. Photobiol. A: Chem. 211 (2010) 185–192.
[31] M.V. Dozzi, L. Prati, P. Canton, E. Selli, Effects of gold nanoparticles deposition on the photocatalytic activity of titanium dioxide under visible light, Phys. Chem. Chem. Phys. 11 (2009) 7171–7180.
[32] L.S. Clesceri, A.E. Greenberg, A.D. Eaton (Eds.), Standard Methods for the Examination of Water and Wastewater, 20th ed., American Public Health Association, Washington, DC, 1998.
[33] R. Kydd, K. Chiang, J. Scott, R. Amal, Low energy photosynthesis of gold–titania catalysts, Photochem. Photobiol. Sci. 6 (2007) 829–832.
[34] M. Mrowetz, A. Villa, L. Prati, E. Selli, Effects of Au nanoparticles on TiO_2 in the photocatalytic degradation of an azo dye, Gold Bull. 40 (2007) 154–160.
[35] S. Sakthivel, M.V. Shankar, M. Palanichamy, B. Arabindoo, D.W. Bahnemann, V. Murugusan, Enhancement of photocatalytic activity by metal deposition: characterization and photonic efficiency of Pt, Au, and Pd deposited on TiO_2 catalyst, Water Res. 38 (2004) 3001–3008.
[36] A. Orlov, D.A. Jefferson, N. Macleod, R.M. Lambert, Photocatalytic properties of TiO_2 modified with gold nanoparticles in the degradation of 4-chlorophenol in aqueous solution, Catal. Lett. 92 (2004) 41–47.
[37] H. Tran, K. Chiang, J. Scott, R. Amal, Understanding selective enhancement by silver during photocatalytic oxidation, Photochem. Photobiol. Sci. 4 (2005) 565–567.
[38] J.A. Navío, J.J. Testa, P. Djedjeian, J.R. Padrón, D. Rodríguez, M.I. Litter, Iron-doped titania powders prepared by a sol–gel method. Part II. Photocatalytic properties, Appl. Catal. A: Gen. 178 (1999) 191–203.
[39] Y. Xu, M.A.A. Schoonen, The absolute energy positions of conduction and valence bands of selected semiconducting minerals, Am. Miner. 85 (2000) 543–556.
[40] Y. Ku, I.-L. Jung, Photocatalytic reduction of Cr(VI) in aqueous solution by UV irradiation with the presence of titanium dioxide, Water Res. 35 (2001) 135–142.
[41] D.C. Hurum, K.A. Gray, T. Rajh, M.C. Thurnauer, Recombination pathways in the Degussa P25 formulation of TiO_2: surface versus lattice mechanisms, J. Phys. Chem. B 109 (2005) 977–980.
[42] A. Di Paola, M. Bellardita, R. Ceccato, L. Palmisano, F. Parrino, Highly active photocatalytic TiO_2 powders obtained by thermohydrolysis of $TiCl_4$ in water, J. Phys. Chem. C 113 (2009) 15166–15174.

[43] J.M. Joseph, H. Destaillats, H.M. Hung, M.R. Hoffmann, The sonochemical degradation of azobenzene and related azo dyes: rate enhancement via Fenton's reactions, J. Phys. Chem. A 194 (2000) 301–307.
[44] H. Park, W. Choi, Effect of TiO_2 surface fluorination on photocatalytic reactions and photoelectrochemical behaviors, J. Phys. Chem. B 108 (2004) 4086–4093.
[45] M. Mrowetz, E. Selli, Enhanced photocatalytic formation of hydroxyl radicals on fluorinated TiO_2, Phys. Chem. Chem. Phys. 7 (2005) 1100–1102.
[46] M. Mrowetz, E. Selli, H_2O_2 evolution during the photocatalytic degradation of organic molecules on fluorinated TiO_2, New J. Chem. 30 (2006) 108–114.
[47] D. Lawless, D. Meisel, N. Serpone, Role of OH radicals and trapped holes in photocatalysis. A pulse radiolysis study, J. Phys. Chem. 95 (1991) 5166–5170.
[48] J.J. Testa, M.A. Grela, M.I. Litter, Experimental evidence in favor of an initial one-electron-transfer process in the heterogeneous photocatalytic reduction of chromium(VI) over TiO_2, Langmuir 17 (2001) 3515–3517.
[49] J.J. Testa, M.A. Grela, M.I. Litter, Heterogeneous photocatalytic reduction on chromium(VI) over TiO_2 particles in the presence of oxalate: involvement of Cr(V) species, Environ. Sci. Technol. 38 (2004) 1589–1594.
[50] J.M. Meichtry, M. Brusa, G. Mailhot, M.A. Grela, M.I. Litter, Heterogeneous photocatalysis of Cr(VI) in the presence of citric acid over TiO_2 particles: relevance of Cr(V)–citrate complexes, Appl. Catal. B: Environ. 71 (2007) 101–107.
[51] Y. Di Iorio, E. San Román, M.I. Litter, M.A. Grela, Photoinduced reactivity of strongly coupled TiO_2 ligands under visible irradiation: an examination of an Alizarin Red@TiO_2 nanoparticulate system, J. Phys. Chem. C 112 (2008) 16532–16538.
[52] M. Mrowetz, E. Selli, Photocatalytic degradation of formic and benzoic acids and hydrogen peroxide evolution in TiO_2 and ZnO water suspensions, J. Photochem. Photobiol. A: Chem. 180 (2006) 15–22.
[53] G. Cappelletti, C.L. Bianchi, S. Ardizzone, Nano-titania assisted photoreduction of Cr(VI). The role of the different TiO_2 polymorphs, Appl. Catal. B: Environ. 78 (2007) 193–201.
[54] H. Li, Z. Bian, J. Zhu, Y. Huo, H. Li, Y. Lu, Mesoporous Au/TiO_2 nanocomposites with enhanced photocatalytic activity, J. Am. Chem. Soc. 129 (2007) 4538–4539.
[55] U. Siemon, D. Bahnemann, J.J. Testa, D. Rodríguez, M.I. Litter, N. Bruno, Heterogeneous photocatalytic reactions comparing TiO_2 and Pt/TiO_2, J. Photochem. Photobiol. A: Chem. 148 (2002) 247–255.